COMPDYN 2015
5th ECCOMAS Thematic Conference on
Computational Methods in Structural Dynamics and Earthquake Engineering
M. Papadrakakis, V. Papadopoulos, V. Plevris (eds.)
Crete Island, Greece, 25–27 May 2015

ANALYSIS OF VIBRO-ACOUSTIC PROPAGATION IN A MOBILE SCREW COMPRESSOR FOR THE DETERMINATION OF EMITTED ACOUSTIC POWER RADIATED OUTSIDE ITS HOUSING

Jan Dupal[1], Jan Vimmr[1], Vítězslav Adámek[1], and Ondřej Bublík[1]

[1]European Centre of Excellence NTIS - New Technologies for the Information Society,
Faculty of Applied Sciences, University of West Bohemia
Univerzitní 8, Pilsen, CZ-306 14, Czech Republic
e-mail: {dupal,jvimmr,vadamek,obublik}@kme.zcu.cz

Keywords: Screw Compressor, Vibro-Acoustics, Helmholtz Equation, Finite Element Method.

Abstract. *The method for a numerical solution of the vibro-acoustic problem in a mobile screw compressor is proposed and in-house 3D finite element (FE) solver is developed. In order to reduce the complexity of the problem, attention is paid to the numerical solution of the acoustic pressure field in the compressor cavity interacting with the linear elastic compressor housing. Propagation of acoustic pressure in the cavity is mathematically described by the Helmholtz equation in the amplitude form and is induced by periodically varying surface velocity of the engine and compressor assembly. In accordance with prescribed boundary conditions, numerical solution of the Helmholtz equation for the distribution of acoustic pressure amplitudes within the cavity is performed using the finite element method on tetrahedral meshes. For the FE discretisation of the elastic compressor housing, a new 6-noded thin flat shell triangular finite element with 21 DOF based on the Kirchhoff plate theory was developed and implemented. The resulting strong coupled system of linear algebraic equations describing the vibro-acoustic problem, i.e., the problem of interaction between the air inside the cavity and the screw compressor housing, is solved numerically by well-known algorithms implemented in MATLAB. By considering two different benchmark test cases, the developed 3D FE solver is successfully verified against the numerical results provided by the professional computational FE system Radioss. Finally, the vibro-acoustic problem is solved in a simplified model of a real mobile screw compressor by prescribing experimentally measured acoustic velocity on the surface of the engine and compressor assembly. The numerical solution is carried out only with the professional computational FE system Radioss as our developed solver is still unable to process large-sized problems without encountering memory limits. Thus, for the assessment of results computed by Radioss, we use results acquired during experimental measurements on a real mobile screw compressor under operating conditions.*

1 INTRODUCTION

Considering customer requirements and the necessity to satisfy hygienic standards, the producers of mobile screw compressors are compelled to minimise the emitted acoustic power and the related noise. The ongoing research is focused on a proposal of suitable and efficient method and its implementation within a 3D finite element (FE) solver for the numerical solution of the acoustic power radiation from screw compressors.

This paper is primarily focused on numerical solution of the vibro-acoustic problem in a simplified model of real mobile screw compressor. Main attention is paid to the acoustic pressure distribution in the compressor cavity interacting with the linear elastic housing of the screw compressor. It is assumed that the propagation of the acoustic pressure in the cavity is induced by periodically varying surface velocity of the engine and compressor assembly, which is known a priori. Since the periodic function can be expressed in the form of a Fourier series, the problem can be solved for a single excitation frequency value and with regards to linearity of the problem the global solution can be derived using a superposition of the harmonic solutions.

The main contribution of the present study, which follows and extends our previous study [1], is the verification of our developed 3D FE solver against the professional computational FE system Radioss and the numerical solution of vibro-acoustic problem in a simplified model of the real mobile screw compressor PDP70, the geometry of which is prepared according to technical drawings provided by the compressor producer ATMOS Chrást, Ltd. Note that due to memory limitations encountered by our solver, the vibro-acoustic problem in the simplified compressor model is numerically solved only by Radioss. In this case, the obtained numerical results are compared with experimental data measured on a real mobile screw compressor under operating conditions.

2 PROBLEM FORMULATION

For the solution of the vibro-acoustic problem in mobile screw compressors, the computational domain is divided into two subdomains: the compressor cavity $\Omega \subset \mathbf{R}^3$ and the elastic compressor housing $\tilde{\Omega} \subset \mathbf{R}^3$, as displayed in Figure 1. The cavity subdomain Ω is bounded by the boundary $\partial\Omega = \Gamma_{in} \cup \Gamma_{out} \cup \Gamma_w \cup \Gamma_t$, where Γ_{in}, Γ_{out} and Γ_w denote the inlet, the outlet and the rigid walls of the computational domain, respectively. The elastic housing $\tilde{\Omega}$ is bounded by boundary $\partial\tilde{\Omega} = \Gamma_f \cup \Gamma_u \cup \Gamma_t$ where Γ_f denotes the boundary with prescribed force loads and Γ_u denotes the boundary with prescribed displacement field. The interface between the two interacting subdomains, i.e., between the cavity Ω and the housing $\tilde{\Omega}$, is denoted as Γ_t.

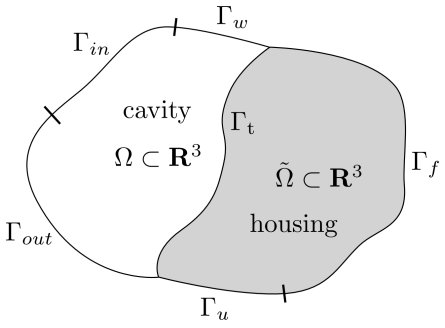

Figure 1: Computational domain $(\Omega \cup \tilde{\Omega}) \subset \mathbf{R}^3$.

Because of the assumption that the excitation is a periodic process, this excitation can be expressed in the form of a Fourier series. Then, with regards to the linearity of the vibro-acoustic problem, its solution, i.e., the distribution of acoustic pressure within the cavity and the distribution of acoustic velocity at the housing surface, can be sought for a single excitation frequency value. Based on this assumption, the acoustic pressure $p'(\boldsymbol{x}, t)$ and the acoustic velocity $\mathbf{v}'(\boldsymbol{x}, t)$ can be expressed in the complex harmonic form $p'(\boldsymbol{x}, t) = p(\boldsymbol{x})e^{i\omega t}$ and $\mathbf{v}'(\boldsymbol{x}, t) = \mathbf{v}(\boldsymbol{x})e^{i\omega t}$, respectively, where ω is the angular frequency of compressor engine movement.

Taking into consideration the harmonic character of the solution, we can write the Helmholtz equation, which describes the distribution of acoustic pressure $p(\boldsymbol{x})$ in the cavity subdomain Ω, in its amplitude form [2]

$$k^2 p + \Delta p = 0, \tag{1}$$

where $k = \frac{\omega}{c}$ is the wave number and c is the speed of sound. In the rest of this paper, all time-dependent variables will be represented by their complex amplitudes. The weak solution of the Helmholtz equation (1) is given as

$$\int_\Omega k^2 \varphi\, p \,\mathrm{d}\Omega - \int_\Omega \nabla\varphi \nabla p \,\mathrm{d}\Omega + \int_{\partial\Omega} \varphi \,\frac{\partial p}{\partial n}\,\mathrm{d}S = 0, \tag{2}$$

where $\varphi(\boldsymbol{x})$ is a well chosen test function and $\boldsymbol{n}$ is the outer unit vector normal to the boundary $\partial\Omega$. The momentum conservation law for the inviscid fluid yields [3]

$$\frac{\partial p}{\partial n} = -i\omega\varrho_a v_n, \tag{3}$$

where i is the imaginary unit, ϱ_a is the air density and $v_n = \boldsymbol{v}\cdot\boldsymbol{n}$ is the normal acoustic velocity. The third integral in Eq. (2) can be expressed for each boundary part as follows:

- the rigid wall boundary Γ_w – the boundary condition $v_n = 0$ is prescribed, which yields $\int_{\Gamma_w} \varphi \,\frac{\partial p}{\partial n}\,\mathrm{d}S = -\int_{\Gamma_w} \varphi\, i\,\omega\varrho_a v_n \,\mathrm{d}S = 0$;
- the anechoic outlet Γ_{out} – the normal velocity v_n is given as [2]

$$v_n = \frac{p}{\varrho_a c}, \tag{4}$$

  which yields $\int_{\Gamma_{out}} \varphi \,\frac{\partial p}{\partial n}\,\mathrm{d}S = -\int_{\Gamma_{out}} \varphi\, i\,\frac{\omega}{c}\, p \,\mathrm{d}S$;
- the inlet boundary Γ_{in} – the surface acoustic velocity v_n is prescribed;
- the interface Γ_t between the cavity and the elastic housing – we apply the following expression $\int_{\Gamma_t} \varphi \,\frac{\partial p}{\partial n}\,\mathrm{d}S = -\int_{\Gamma_t} \varphi\, i\,\omega\varrho_a v_n \,\mathrm{d}S$, where the normal acoustic velocity v_n is an unknown velocity resulting from the interaction between the acoustic environment in the cavity and the elastic housing of the screw compressor.

By including the integrals mentioned above into Eq. (2), we obtain the following equation

$$\int_\Omega k^2 \varphi\, p \,\mathrm{d}\Omega - \int_\Omega \nabla\varphi \nabla p \,\mathrm{d}\Omega - i\,\frac{\omega}{c}\int_{\Gamma_{out}} \varphi\, p \,\mathrm{d}S - i\omega\varrho_a \int_{\Gamma_{in}} \varphi\, v_n \,\mathrm{d}S - i\omega\varrho_a \int_{\Gamma_t} \varphi\, v_n \,\mathrm{d}S = 0. \tag{5}$$

Note that the normal velocity v_n in the fourth integral is given, whereas in the fifth integral it is unknown.

The solution in the housing subdomain $\tilde{\Omega}$ is based on the principle of virtual work (PVW) in the following form

$$\int_{\tilde{\Omega}} \delta\boldsymbol{\varepsilon}^T \boldsymbol{\sigma} \,\mathrm{d}\tilde{\Omega} = -\int_{\tilde{\Omega}} \varrho_h \delta\boldsymbol{u}^T \ddot{\boldsymbol{u}} \,\mathrm{d}\tilde{\Omega} + \int_{\Gamma_t} p\, \delta\boldsymbol{u}^T \boldsymbol{n} \,\mathrm{d}S, \tag{6}$$

where $\boldsymbol{\varepsilon} = [\varepsilon_x, \varepsilon_y, \varepsilon_z, \gamma_{yz}, \gamma_{xz}, \gamma_{xy}]^T$ is the strain vector, $\boldsymbol{\sigma} = [\sigma_x, \sigma_y, \sigma_z, \tau_{yz}, \tau_{xz}, \tau_{xy}]^T$ is the stress vector, $\boldsymbol{u} = [u, v, w]^T$ is the displacement vector and ϱ_h is the material density of the housing. The surface integrals over the boundary Γ_u with prescribed zero displacements and Γ_f with prescribed zero loads are equal to zero and are therefore omitted from Eq. (6).

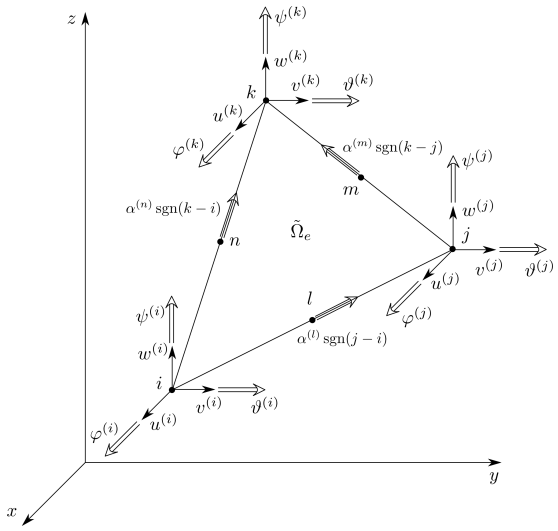

Figure 2: Six-noded thin flat shell triangular finite element $\tilde{\Omega}_e$ after transformation.

3 FINITE ELEMENT DISCRETISATION

If we consider the Helmholtz equation for the cavity in the weak form (5) and the equation of motion (6) for the housing in the amplitude form for the given excitation frequency, then the solution of both aforementioned equations will take the form of complex pressure amplitudes within the cavity and velocity amplitudes at the housing surface.

The FE discretisation of the Helmholtz equation, describing the distribution of acoustic pressure amplitudes within the cavity subdomain $\Omega \subset \mathbf{R}^3$, was carried out using a tetrahedral 3D finite element described in [1]. For the FE discretisation of the housing subdomain $\tilde{\Omega} \subset \mathbf{R}^3$, a new 6-noded thin flat shell triangular finite element $\tilde{\Omega}_e$ with 21 degrees of freedom (DOF) was developed. The proposed thin flat shell element is based on the Kirchhoff plate theory [4]. After transformation, each corner node i, j and k contains three displacements u, v, w and three rotations φ, ϑ and ψ. The midside nodes l, m and n store the information about the rotation angle around the element edge, where the sense of rotation is determined by the sign of difference of numbers of the corresponding edge corner nodes, see Figure 2. For more details, see [1].

The FE discretisation of both the cavity and the housing subdomains yields the following equation describing their interaction in the vibro-acoustic problem solved in this paper

$$\begin{bmatrix} i\omega\mathbf{H} + \mathbf{G} + \frac{1}{i\omega}\mathbf{F} & \mathbf{Z} \\ \mathbf{Z}^T & i\omega\mathbf{M} + \mathbf{B} + \frac{1}{i\omega}\mathbf{K} \end{bmatrix} \begin{bmatrix} \mathbf{p} \\ \dot{\mathbf{q}} \end{bmatrix} = \begin{bmatrix} \mathbf{A}_f\mathbf{v}^{in} \\ \mathbf{f} \end{bmatrix}, \tag{7}$$

where $\mathbf{M}$, $\mathbf{B}$ and $\mathbf{K}$ are the matrices of mass, damping and stiffness, respectively. In the case of the cavity subdomain (the upper part of Eq. (7)), the coupling matrix $\mathbf{Z}$ represents the boundary condition of normal velocity shared by the cavity boundary and the housing subdomain (the fifth term in Eq. (5)). In the case of the housing subdomain, it corresponds to the pressure exerted by the cavity on the housing. The matrices $\mathbf{H}$ and $\mathbf{F}$ are the result of FE discretisation of the first two terms in Eq. (5), which describe the distribution of acoustic pressure amplitudes within the cavity without the influence of boundary conditions. The application of the anechoic outlet boundary condition yields the matrix $\mathbf{G}$, which corresponds to the third term in Eq. (5) and expresses the fact that the acoustic wave is reflection-free. The prescription of given velocity amplitudes at the inlet leads to $\mathbf{A}_f\mathbf{v}^{in}$, which corresponds to the fourth term in Eq. (5). The

vector $\mathbf{f}$ is the complex amplitude vector of external forces exerted on the housing subdomain. Note that the derivation of the matrices appearing in Eq. (7) was demonstrated in the paper [1] for one finite element. The global matrices are assembled using a standard FEM procedure.

The resulting emitted acoustic power can be computed from normal acoustic velocities and amplitudes of acoustic pressure defined in points located at the housing surface. The amplitudes of acoustic pressure can be determined from the condition of anechoic outlet (4) applied to the outer surface of the housing subdomain Γ_t. Then, for the emitted acoustic power, it holds

$$P_{acoustic} = \int_{\Gamma_t} \boldsymbol{v} \cdot \boldsymbol{n}\, p \,\mathrm{d}S = \int_{\Gamma_t} v_n\, p \,\mathrm{d}S \overset{\text{Eq.(4)}}{=} \int_{\Gamma_t} v_n^2\, \varrho_a\, c \,\mathrm{d}S. \tag{8}$$

4 NUMERICAL RESULTS

The proposed methodology for the numerical solution of vibro-acoustic problems in mobile screw compressors was implemented in our in-house 3D FE solver developed in MATLAB. The computational ability of this solver was tested on two examples – test cases No.1 a No.2 described in Sections 4.1 and 4.2.

4.1 Test case No.1

The numerical solution of the vibro-acoustic problem was first carried out for a test computational domain, the geometry of which was that of a $1 \times 0.7 \times 0.5\,\mathrm{m}$ block shown in Figure 3. The bottom of the computational domain was assumed to be perfectly rigid and corresponding to the cavity subdomain boundary Γ_w. The remaining walls of the computational domain formed the interface Γ_t between the cavity and the elastic structure (housing), which was made of a thin metal sheet with thickness of $1\,\mathrm{mm}$, density $\varrho_h = 7\,800\,\mathrm{kg/m^3}$, Young's modulus $E = 2.1 \times 10^{11}\,\mathrm{Pa}$ and Poisson ratio $\mu = 0.3$. Within the cuboidal cavity, there was another smaller perfectly rigid block $(0.1 \times 0.2 \times 0.2\,\mathrm{m})$, Figure 3, situated $0.1\,\mathrm{m}$ above the bottom of the computational domain. At the upper and lower walls (domain boundary Γ_{in}) of the smaller block, we prescribed a normal velocity $v_n \equiv v_y$ with amplitude $0.05\,\mathrm{m/s}$ and excitation frequency $f = 100\,\mathrm{Hz}$. At the side walls, zero normal velocity v_n was given. The density of air within the cavity was set equal to $\varrho_a = 1.2\,\mathrm{kg/m^3}$ and the speed of sound was assumed to be $c = 340\,\mathrm{m/s}$. In this test case, the system without damping was considered. The space discretisation of the cavity for the developed 3D FE solver as well as the professional computational FE system Radioss was carried out for an unstructured tetrahedral mesh consisting of around 15 000 elements with edge lengths around $5\,\mathrm{cm}$, Figure 7 (right). Moreover, the solution in Radioss also required the elastic structure (housing) to be discretised with around 2 700 thin shell elements, the size of which was approximately the same as in the case of the cavity mesh.

Figure 4 shows the distribution of acoustic pressure amplitudes in the axial longitudinal section of the cavity subdomain computed by the developed 3D FE solver. This acoustic pressure distribution was compared with the results provided by the professional computational FE system Radioss using the modal approach for the solution of the considered vibro-acoustic problem. The computations in the system Radioss were carried out for different numbers of eigenfrequencies and eigenmodes of the cavity and the elastic structure considered by the computation of the system response. As expected, the obtained numerical results showed that both the distribution of the acoustic pressure in the cavity and the distribution of the acoustic velocity at the structure surface are dependent on the number of considered eigenmodes. Taking into consideration the computed maximum values of acoustic pressure, this dependency is well

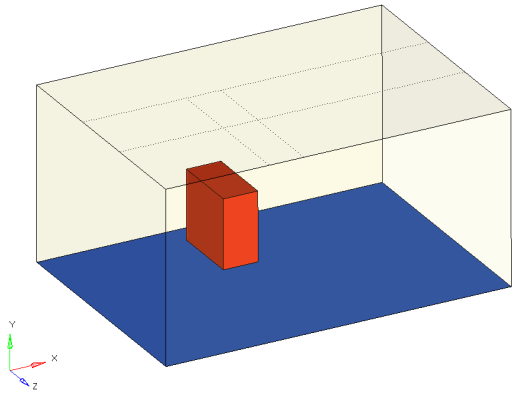

Figure 3: Geometry of the computational domain considered in the test case No.1.

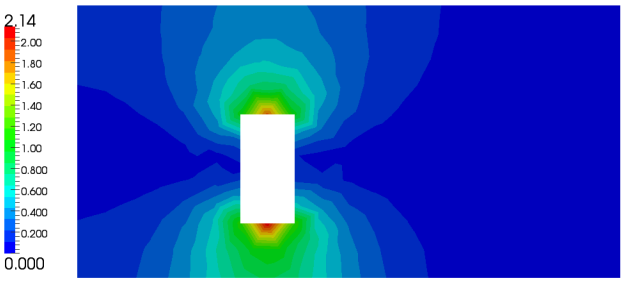

Figure 4: Acoustic pressure amplitudes in the axial longitudinal section of the cavity computed by the developed 3D FE solver.

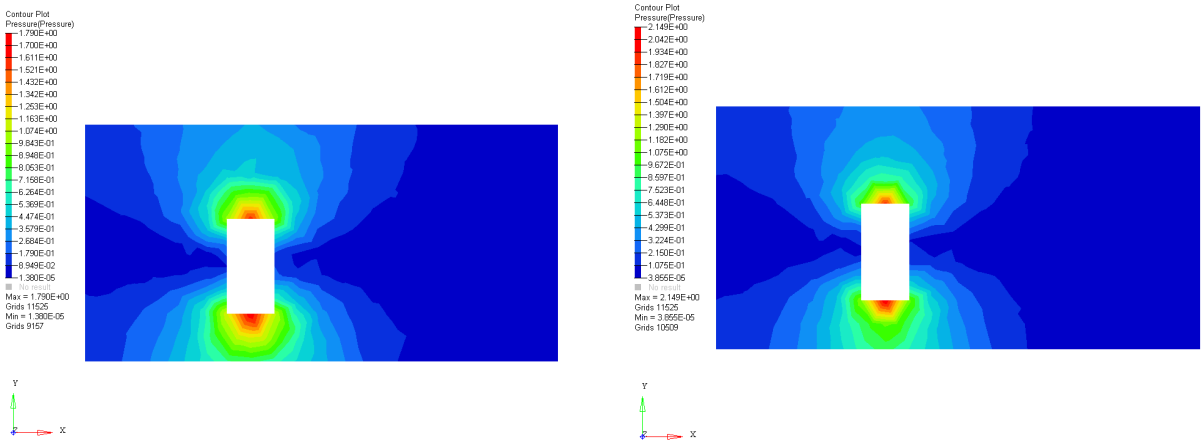

Figure 5: Acoustic pressure amplitudes in the axial longitudinal section of the cavity computed by the professional FE system Radioss for 1 000 and 50 (*left*) and 2 000 and 100 (*right*) cavity and structure eigenmodes.

No. of eigenmodes		
cavity	structure	p_{max} [Pa]
200	200	1.126
500	200	1.433
1 000	200	1.790
1 000	500	1.791
2 000	500	2.149
1 000	100	1.790
1 000	50	1.790
3 000	50	2.118
2 000	100	2.149

Table 1: Number of cavity and structure eigenmodes with corresponding maximum pressure amplitudes p_{max}.

apparent from Table 1. With the help of the developed direct 3D FE solver, the maximum acoustic pressure was determined as 2.14 Pa, see Figure 4. From Table 1, it can be also noted that in order to achieve an acoustic pressure amplitude comparable with the one provided by the developed direct 3D FE solver, it is necessary to consider at least 2 000 eigenmodes of the

cavity and 100 eigenmodes of the structure. The eigenfrequencies corresponding to the 2 000th eigenmode of the cavity and the 100th eigenmode of the structure are 2.67 kHz and 180 Hz. Figure 5 shows the distribution of acoustic pressure amplitudes in the axial longitudinal section of the cavity computed by the professional computational FE system Radioss for the combination of 1 000 and 50 or 2 000 and 100 cavity and structure eigenmodes. By comparing Figure 4 and Figure 5 (right), it is possible to observe that the results computed by the developed 3D FE solver and the professional computational FE system Radioss are in relatively good agreement when the combination of 2 000 and 100 eigenmodes is taken into consideration. A similarly good agreement between both solvers could be achieved for the computation of acoustic velocity amplitudes at the surface of the elastic structure, as apparent from Figures 6 and 7. The maximum velocity amplitude computed by the developed 3D FE solver was $2.25 \times 10^{-4}\,\mathrm{m/s}$, Figure 6, while the professional FE solver Radioss provided a value of $2.03 \times 10^{-4}\,\mathrm{m/s}$, see Figure 7 (right).

In accordance with Eq. (8), the emitted acoustic power was computed as $2.1663 \times 10^{-6}\,\mathrm{W}$.

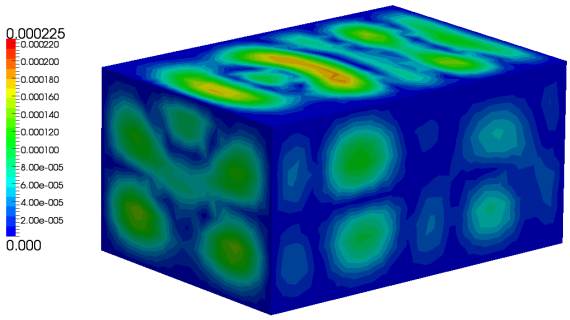

Figure 6: Velocity amplitudes at the surface of the elastic structure computed by the developed 3D FE solver.

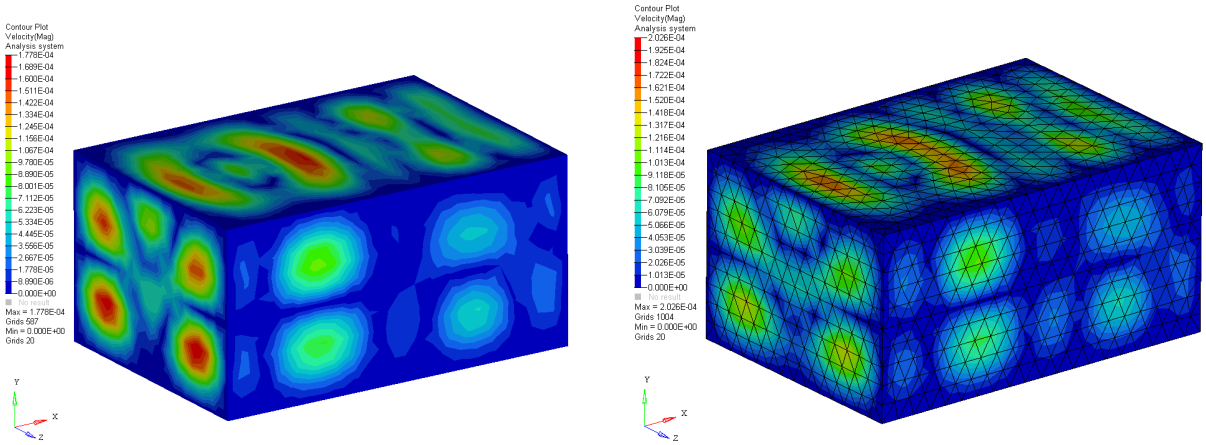

Figure 7: Velocity amplitudes at the surface of the elastic structure computed by the professional FE system Radioss for 1 000 and 50 (*left*) and 2 000 and 100 (*right*) cavity and structure eigenmodes.

4.2 Test case No.2

Following the previous test case, the vibro-acoustic problem was numerically solved in a $2.6 \times 1.3 \times 1.1$ m test computational domain, the geometry of which corresponded to the housing of a real mobile screw compressor, Figure 8. The numerical solution was carried out under

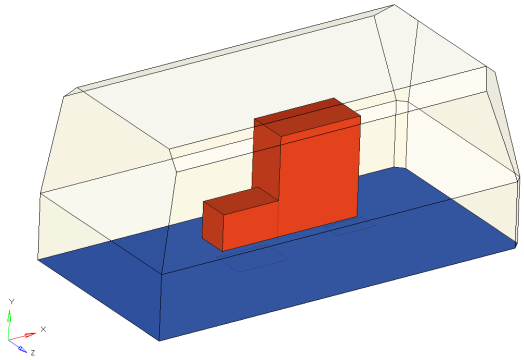

Figure 8: Geometry of the computational domain considered in the test case No.2.

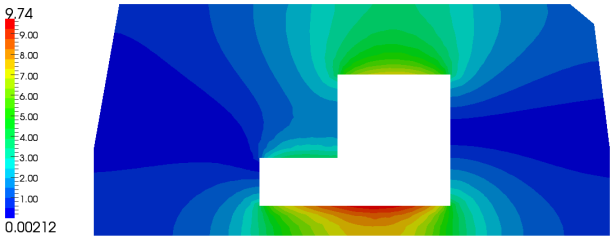

Figure 9: Acoustic pressure amplitudes in the central longitudinal section of the cavity computed by the developed 3D FE solver.

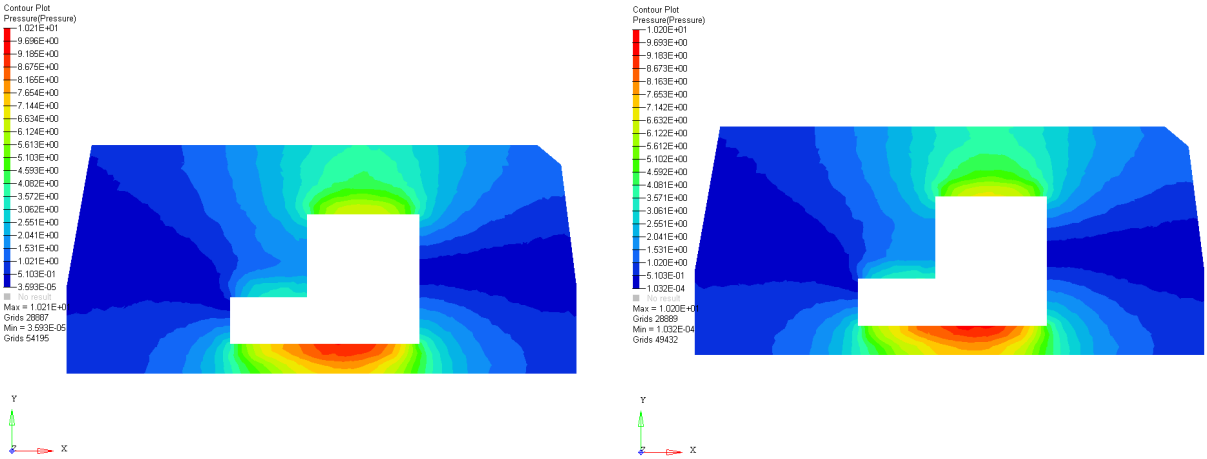

Figure 10: Acoustic pressure amplitudes in the axial longitudinal section of the cavity computed by the professional FE system Radioss for 2 000 and 100 (*left*) and 5 000 and 400 (*right*) cavity and structure eigenmodes.

the same conditions and assumptions as in the previous test case, with the only exception that the size and position of the excitation source now better reflected the size and position of the real engine and compressor assembly within the cavity. Once again the normal velocity $v_n \equiv v_y$ was prescribed at the upper and lower walls of the assembly, while the amplitude and frequency were chosen to be the same as in the previous test case. The space discretisation of the cavity for the developed 3D FE solver as well as the professional computational FE system Radioss was carried out for an unstructured tetrahedral mesh consisting of approximately 151 000 tetrahedral elements with edge lengths around 5 cm, see Figure 12 (right). The solution in Radioss additionally required the elastic structure (housing) to be discretised with around 13 500 thin shell elements, the size of which was approximately the same as in the case of the cavity mesh.

Figure 9 shows the distribution of acoustic pressure amplitudes in the axial longitudinal section of the cavity computed by the developed direct FE solver. Similarly to the previous test case, this distribution was compared with the one provided by the professional FE system Radioss, see Figure 10. The left picture in Figure 10 shows the distribution of acoustic pressure amplitudes computed for considered 2 000 cavity and 100 structure eigenmodes. Note that the eigenfrequencies of the system corresponding to the 2000th cavity and the 100th structure eigenmodes were 1.54 kHz and 52 Hz, respectively. The combination of 5 000 cavity and 400 structure eigenmodes is shown in Figure 10 (right). Here, the corresponding eigenfrequencies

were stated to be 1.94 kHz a 158 Hz. As can be noted from Figure 10, the distribution of acoustic pressure amplitudes is almost identical in both eigenmode combinations, especially when they yielded the same maximum acoustic pressure of 10.2 Pa. The results are in very good agreement with the ones computed by the developed direct FE solver, Figure 9, which provided maximum acoustic pressure of 9.74 Pa. A good result agreement between the developed FE solver and the professional FE system Radioss could be also achieved by the computation of acoustic velocity amplitudes at the housing surface, as seen when comparing Figures 11 and 12 (right). The maximum velocity amplitude computed by the developed FE solver was $2.43 \times 10^{-3}\,\mathrm{m/s}$, Figure 11, while the professional FE system Radioss provided a value of $2.31 \times 10^{-3}\,\mathrm{m/s}$ when the combination of 5 000 cavity and 400 structure eigenmodes was taken into consideration, Figure 12 (right). From Figure 12 (left), it is well apparent that the combination of 2 000 cavity and 100 structure eigenmodes (this modal reduction) is not suitable for the computation of acoustic velocities, even though it is able to provide a distribution of acoustic pressure amplitudes that is comparable with that computed by the developed direct FE solver.

In accordance with Eq. (8), the emitted acoustic power was computed as $4.044 \times 10^{-4}\,\mathrm{W}$.

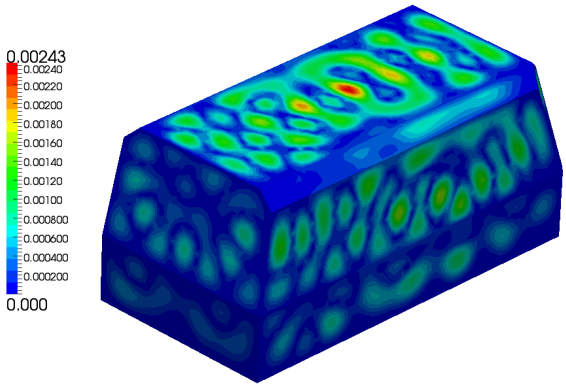

Figure 11: Velocity amplitudes at the housing surface computed by the developed 3D FE solver.

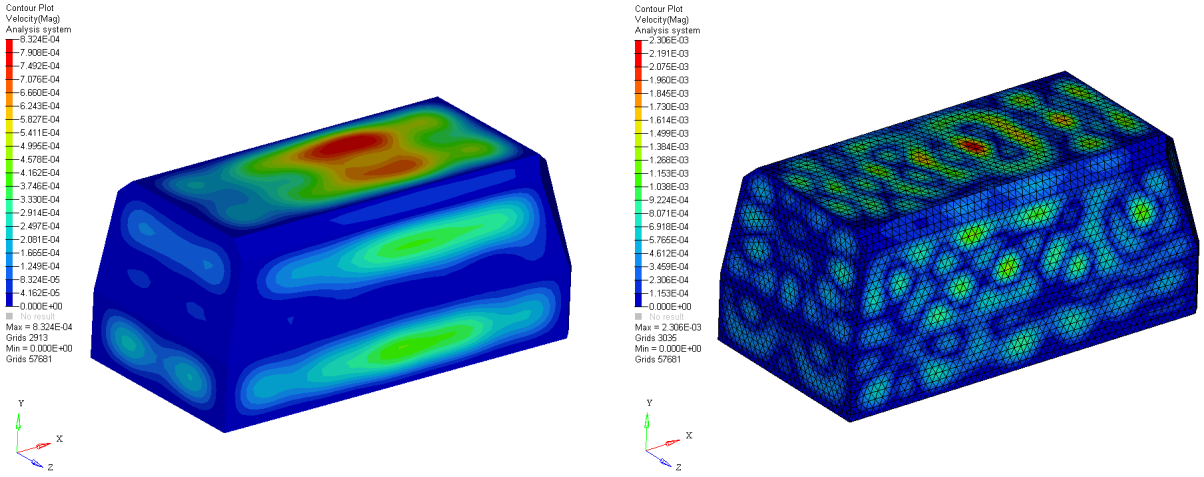

Figure 12: Velocity amplitudes at the housing surface computed by the professional FE system Radioss for 2 000 and 100 (*left*) and 5 000 and 400 (*right*) cavity and structure eigenmodes.

4.3 Vibro-acoustic problem in a simplified model of real mobile screw compressor

By using the professional computational FE system Radioss, the numerical solution of the vibro-acoustic problem is carried out in a computational domain that represents a simplified model of the real mobile screw compressor PDP70, Figure 13 (left), the geometry of which was prepared according to the technical drawings provided by the compressor producer ATMOS Chrást, Ltd. The bottom of the computational domain was assumed to be perfectly rigid and corresponding to the cavity subdomain boundary Γ_w. The cavity contained the most significant compressor components such as the pressure vessel of the oil separator, the fuel tank, the battery and the fan cover, Figure 13 (right), which were all connected to the cavity bottom. The cavity subdomain was surrounded by an elastic wall made of a thin metal sheet with thickness of 1.5 mm and enforced by stiffening ribs with thickness between 1.5 and 3 mm (the housing of the compressor). The presence of the stiffening ribs is well apparent in Figure 13. In this vibro-acoustic problem, the source of excitation was the engine and compressor assembly, which was once again assumed to be rigid. The surface of this assembly corresponded to the domain boundary Γ_{in} with prescribed acoustic velocity. Experimental measurements of velocity were performed at this surface at three points denoted as M1, M6 and M20, see Figure 13 (right). The Fourier spectrum of velocity components measured at the aforementioned points is shown in Figure 14 for the excitation frequency range between 20 Hz to 2 kHz. With regard to the fact that a rigid body has 6 DOF, the number of prescribed velocity components at each of the three points was chosen as follows: v_x, v_y, v_z at M1, v_y, v_z at M6 and v_z at M20. The material parameters used for the numerical solution of this vibro-acoustic problem were taken the same as in the previous two test cases. However, compared to the two test cases, the current problem considered a damped system. The space discretisation of the cavity was carried out by using an unstructured mesh consisting of around 1 800 000 tetrahedral elements, while the housing was discretised with almost 120 000 thin shell elements, the size of which was approximately 2 cm.

Using the modal approach in the professional computational FE system Radioss, the numerical solution of the vibro-acoustic problem was carried out up to the eigenfrequency of 2 kHz for both the cavity and the compressor housing. This eigenfrequency threshold corresponds to the 3164th and the 4708th considered eigenmodes of the cavity and the elastic structure (housing), respectively. The results of the numerical solution consisted of the complex amplitudes of acoustic pressure within the cavity and the complex amplitudes of acoustic velocity at the hous-

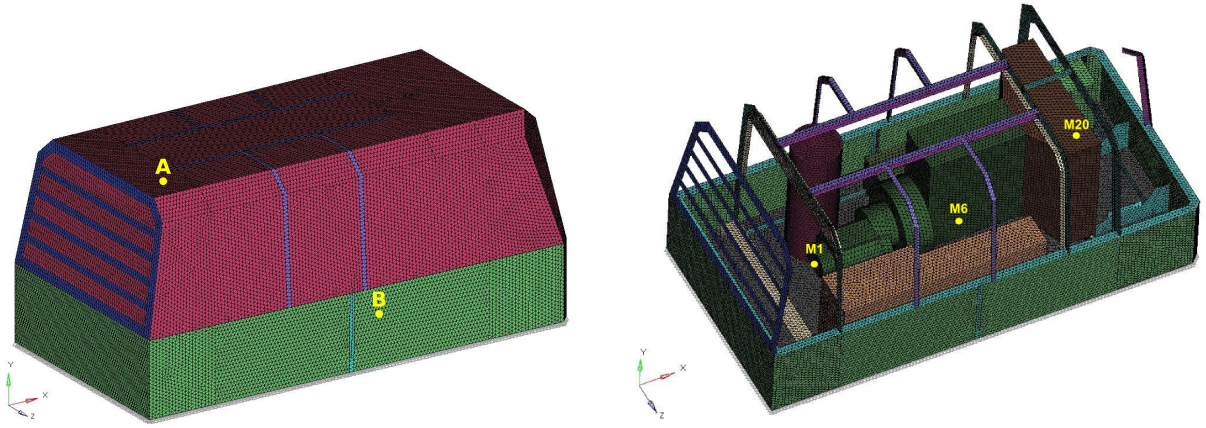

Figure 13: Simplified model of a real mobile screw compressor – housing (*left*) and cavity with the most significant components (*right*).

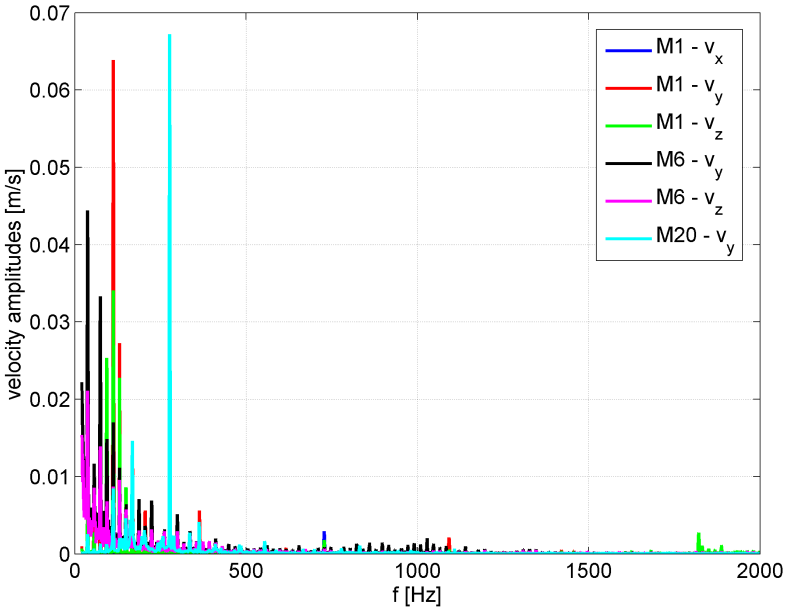

Figure 14: Fourier spectrum of velocity components measured at the points shown in Figure 13 (right).

ing surface, computed for each excitation frequency. Figure 15 shows the obtained distributions of acoustic pressure amplitudes in selected sections of the cavity for the excitation frequencies 1 kHz and 2 kHz. The final distribution of acoustic pressure amplitudes after the superposition over all excitation frequencies, which were taken in accordance with the frequency range considered during the experimental measurements (Figure 14), is shown in Figure 16.

In the same context as in the case of acoustic pressure amplitudes, Figures 17 and 18 show the distributions of amplitudes of the acoustic velocity components v_y and v_z, respectively, at the housing surface for the excitation frequencies 1 kHz and 2 kHz. The resulting amplitude distribution of both aforementioned acoustic velocity components after the superposition over all excitation frequencies, which were taken in accordance with the frequency range considered during the experimental measurements (Figure 14), is visualised in Figure 18.

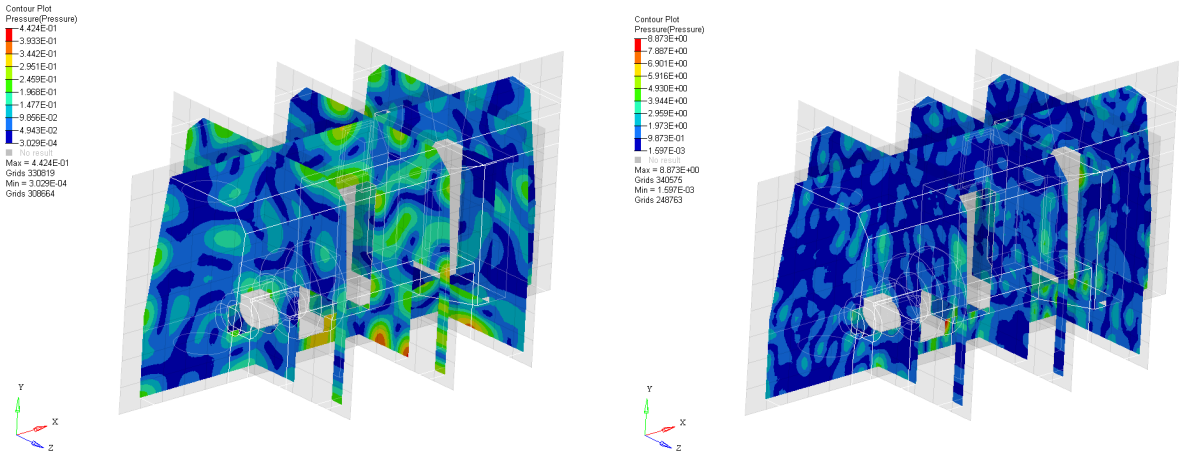

Figure 15: Acoustic pressure amplitudes in selected sections of the cavity computed by the professional FE system Radioss for the excitation frequencies 1 kHz (*left*) and 2 kHz (*right*).

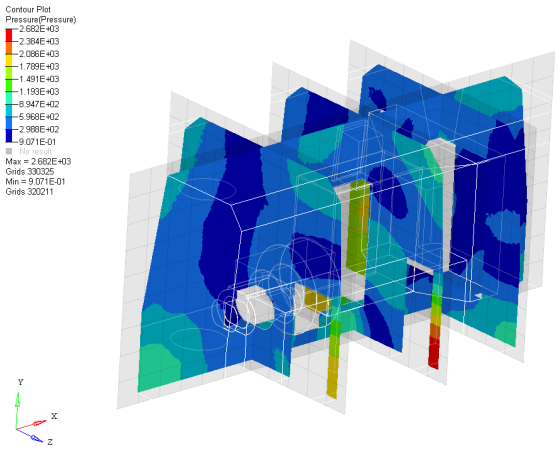

Figure 16: Acoustic pressure amplitudes in selected sections of the cavity after the superposition over all excitation frequencies.

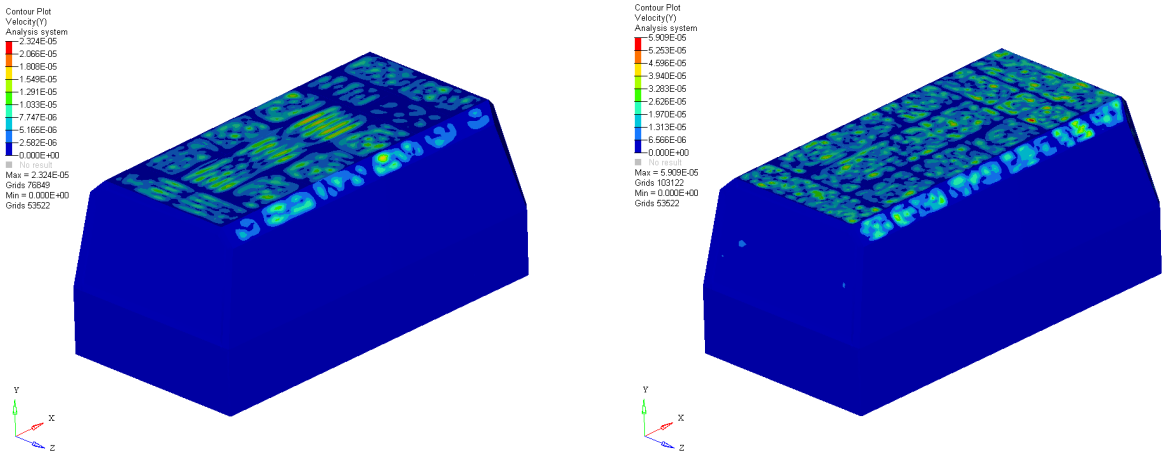

Figure 17: Amplitudes of the acoustic velocity component v_y at the housing surface computed by the professional FE system Radioss for the excitation frequencies 1 kHz (*left*) and 2 kHz (*right*).

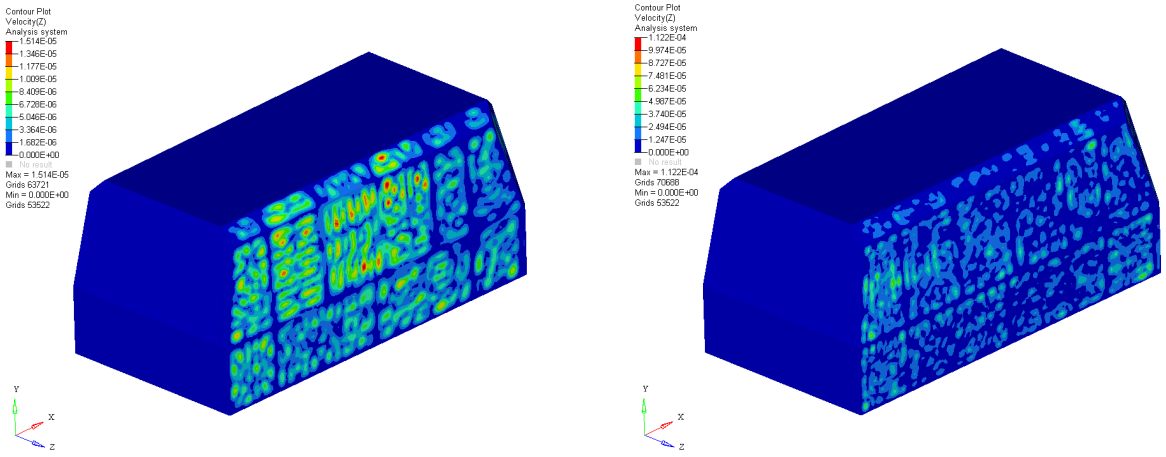

Figure 18: Amplitudes of the acoustic velocity component v_z at the housing surface computed by the professional FE system Radioss for the excitation frequencies 1 kHz (*left*) and 2 kHz (*right*).

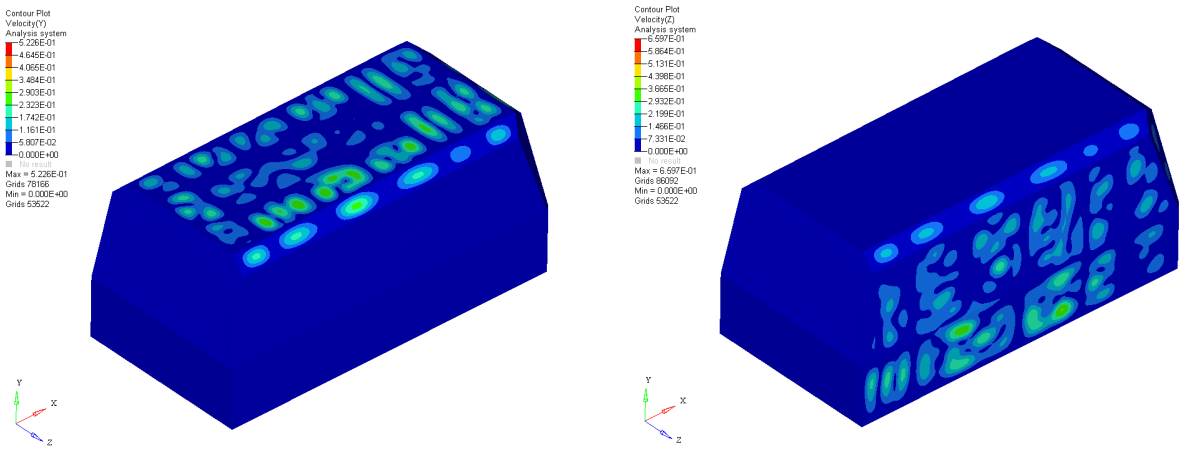

Figure 19: Amplitudes of the acoustic velocity components v_y (*left*) and v_z (*right*) after the superposition over all excitation frequencies.

A comparison of computed and measured acoustic velocity components v_y in the frequency domain was carried out for one selected point located on the housing roof (denoted by A in Figure 13 (left)) with the result shown in Figure 20. Analogously, Figure 21 provides the comparison of computed and measured acoustic velocity components v_z in the frequency domain for one selected point located on the housing side (denoted by B in Figure 13 (left)). On the basis of both comparisons, it can be noted that a good agreement between the computed and measured values was not reached. By taking into consideration the fact that the experimental measurements were carried out on a real mobile screw compressor under operating conditions, it is possible to deduce several factors that may have caused the observed differences. The first one is related to the simplified geometry of the cavity space, which did not include all of the components found in the real screw compressor, such as pressure hoses and cables. A certain influence on the computed results can be also attributed to the applied geometry of the engine and compressor assembly, which was simplified to the maximum possible extent. Although the

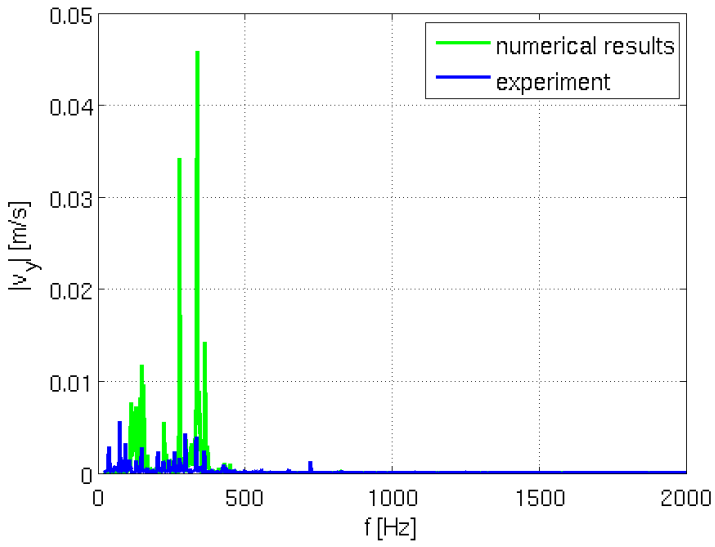

Figure 20: Comparison of computed and measured acoustic velocity components v_y in the frequency domain for the point A denoted in Figure 13 (left).

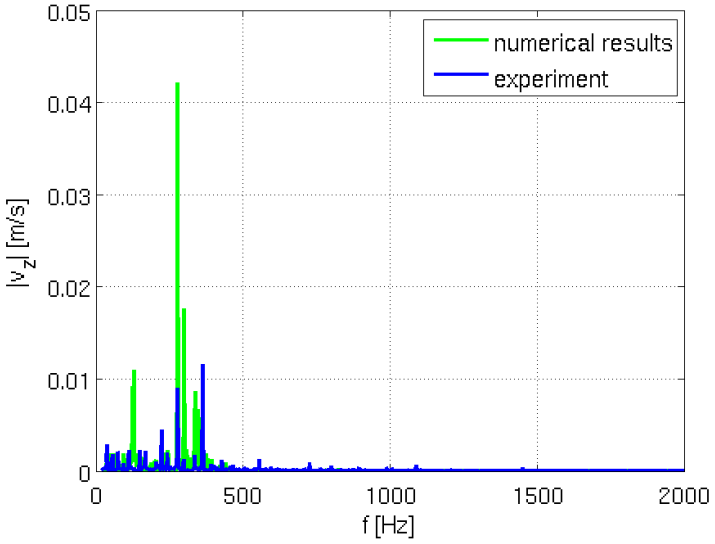

Figure 21: Comparison of computed and measured acoustic velocity components v_z in the frequency domain for the point B denoted in Figure 13 (left).

aforementioned simplifications certainly played a role in the disagreement between the computed and measured values, they were probably not the main cause. The reason why there are differences between the numerical and experimental data is most likely due to the computation of acoustic pressure within the cavity and housing vibrations, which were taken as a result of acoustic wave propagation from the engine and compressor assembly to the housing via the cavity. In reality, the housing vibrations are strongly influenced by the direct transmission of vibrations from the assembly to the housing through their joints. Compared to the performed experiments, the transmitted vibration was not considered in the present numerical study. Another cause of dissimilarities between the computed and measured results was the assumption that the engine and compressor assembly, including other cavity components, were modelled as rigid, even though in reality they are compliant to a certain extent.

5 CONCLUSIONS

For the FE discretisation of the compressor housing subdomain carried out in this study, a new 6-noded thin flat shell triangular finite element with 21 DOF (6 DOF in corner nodes and 1 DOF in each element midside) was developed and implemented in the developed 3D FE solver for the numerical solution of vibro-acoustic problems in mobile screw compressors. The correctness of the developed flat shell finite element, the proposed methodology and the developed FE solver were verified for two test cases described in this study. The verification was carried out by comparing amplitudes of acoustic pressure within the cavity and amplitudes of acoustic velocity at the surface of the elastic structure (housing) computed by the developed direct FE solver with those provided by the modal approach of the professional FE system Radioss. A very good agreement between both FE solvers was achieved in both test cases. The development of our in-house FE solver is motivated by our effort to acquire a code open for future changes and modifications that would enable a consequent parameter optimisation aimed at the elimination or minimisation of the emitted acoustic power. In this case, the optimisation process could include a sensitivity analysis to determine how changes in the geometry and material parameters can affect the emitted noise. The considered test cases also revealed that

the developed direct FE solver was almost three times faster than the professional one when run on the same computer.

Unfortunately, due to high memory demands, the direct FE solver developed in MATLAB is not capable to solve large vibro-acoustic problems discretised to contain more than 1 500 000 finite elements. It is, therefore, understandable that our future efforts regarding the solver improvement will be oriented towards memory usage optimisation. The aforementioned high memory demands are the main reason why the numerical solution of the vibro-acoustic problem involving the simplified model of real mobile screw compressor, was carried out only by the professional FE system Radioss. To assess the numerical results, we compared them with the experimental data provided by measurements carried out under operating conditions on the real mobile screw compressor PDP70 produced by the company ATMOS Chrást, Ltd. As already discussed in Section 4.3, the observed differences in results were mainly caused by the following factors, which can be seen as the limitations of the study:

- The experimental data included vibrations caused by energy transmission between the engine and compressor assembly and the housing via their joints. Compared to this, our study respected the vibration transmission between the aforementioned components only through the acoustic component, i.e., the observed vibrations were the result of acoustic wave propagation from the assembly surface to the surrounding housing via the compressor cavity.
- Compared to the reality, the present study also adopted the simplification that the engine and compressor assembly, including other components situated within the cavity, were assumed to be rigid. Moreover, the experimental data only contained information on the measured amplitude spectra of velocity components and did not provide the corresponding phase.
- In this study, the real geometry of the cavity subdomain was considerably simplified by omitting components such as pressure hoses and electrical cables. The shape of the engine and compressor assembly was simplified, as well.

ACKNOWLEDGEMENTS

This study was supported by the European Regional Development Fund (ERDF), project NTIS – New Technologies for the Information Society, European Centre of Excellence, CZ.1.05/1.1.00/02.0090. The authors of this study would like to thank the company ATMOS Chrást, Ltd., which as a compressor producer provided the necessary technical drawings. The experimental data used for the purpose of this study were acquired by Ing. Oldřich Tureček, Ph.D. and Ing. Martin Sýkora, Ph.D. from the Faculty of Electrical Engineering, University of West Bohemia, whose help is thereby gratefully acknowledged. The assistance of Ing. Alena Jonášová, Ph.D. during the preparation of the manuscript is acknowledged, as well.

REFERENCES

[1] J. Dupal, J. Vimmr, O. Bublík, M. Hajžman, Modelling of acoustic power radiation from mobile screw compressors. Z. Dimitrovová et al. eds. *11th International Conference on Vibration Problems*, Lisbon, Portugal, September 9-12, 2013.

[2] L.E. Kinsler, A.R. Frey, A.B. Coppens, J.V. Sanders, *Fundamentals of acoustics, 4th Edition*. John Wiley & Sons, Inc., 2000.

[3] S. Temkin, *Elements of acoustics*. Acoustical Society of America, 2001.

[4] E. Oñate, *Structural analysis with the finite element method. Linear statics. Volume 2 – Beams, plates and shells*. Lecture Notes on Numerical Methods in Engineering and Sciences, CIMNE, 2013.